Thermophoresis of highly absorbing, emitting particles in laminar tube flow

S. J. Yoa and S. S. Kim
Department of Mechanical Engineering, Korea Advanced Institute of Science and Technology, Seoul, Korea

J. S. Lee
Department of Mechanical Engineering, Seoul National University, Seoul, Korea

The effect of radiation on the thermophoresis phenomenon owing to the presence of highly absorbing, emitting particles (such as soot or pulverized coal) suspended in a two-phase flow system is investigated numerically for a laminar tube flow. The analysis of conservation equations for a gas–particle flow system is performed on the basis of a two-fluid model from a continuum Eulerian viewpoint. In addition, the P-1 approximation is used to evaluate radiation heat transfer. Under a strong radiative effect, the rate of thermophoretic particle deposition becomes considerably less. The effects of the thermal loading ratio and the Stokes number on thermophoresis phenomenon also are examined.

Keywords: two-fluid model; thermophoresis; cumulative collection efficiency

Introduction

The study of particle transport in a gas–solid two-phase flow is of great importance in many engineering applications. The fabrication of optical wave guides and semiconductor devices and the successful design of many types of equipment, such as heat exchangers, require an understanding of the mechanism of mass transfer from particle or droplet-laden gas streams to solid surfaces. The transport of heavy molecules and particles may be described as several different mechanisms (e.g., thermophoresis, inertial impaction, Brownian diffusion, etc.). In terms of Brownian diffusion, this effect is usually negligible because the Brownian diffusivity of particles is very small relative to gas diffusivity. The reason is the massive size of a particle compared to a gas molecule.[1,2] Additionally, Brownian coagulation can be an important mechanism for particle transport in an aerocolloidal system.[2] Coagulation is a strong function of particle concentration, particle size, and process residence time; that is, a criterion at which Brownian coagulation occurs, can be represented by the ratio of the coagulation characteristic time to the process residence time.[3,4] Brownian coagulation is negligible when the coagulation characteristic time is much longer than the process residence time. Particle movement is therefore primarily affected by fluid convection and thermophoresis. Sometimes, in a nonisothermal gas–solid mixture system, inertial impaction can be coupled with thermophoresis as the Stokes number increases.

As investigated experimentally by Fulford *et al.*,[5] Derjaguin *et al.*,[6] Goldsmith and May,[7] and Rosner and Kim,[8] the thermophoresis phenomenon is important for particles as large as 10 μm and temperature gradient of the order of 50 K/cm (i.e., proportional to $-$gradient (ln T), which produces the net thermophoretic transport). Moreover, in the presence of highly absorbing, emitting particles such as soot, fly ash, and pulverized coal, which significantly alter the temperature field of a gas–solid mixture, the radiation effect on thermophoresis becomes important since thermophoresis is strongly dependent on the temperature gradient.[9]

So far, most of the experimental or numerical studies of the thermophoresis phenomenon have neglected the radiation effect. Experimentally, thermophoretic deposition has been studied in laminar gas streams by Derjaguin *et al.*[6] for particles up to about 5 μm in diameter, Goldsmith *et al.*[7] for small particles, and in a turbulent pipe flow by Calvert and Byers.[10] Also, the thermophoretic transport of particles in channel flows and boundary layer flows over a flat plate has been studied analytically or numerically by Goren,[9] Epstein *et al.*,[11] and others, and in tube flow by Walker *et al.*[12] Most investigators have utilized low-absorbing materials, such as glass beads, TiO_2, and MgO, for particulate phase in a two-phase flow system. In particular, Morse *et al.*[13] and Cipolla and Morse[14] have considered absorbing, nonemitting aerosol under low enclosure temperature when the particle is produced by laser heating in the MCVD process. However, when a gas–solid mixture including soot, fly ash, and coal as undesirable by-products is a moving fluid in a heat exchanger or an internal combustion chamber, this flow system may contribute greatly to radiation.

Therefore, in the case of seeding highly absorbing particles into gas streams, any analysis of particle diffusion in non-isothermal gas that neglects the radiation effect for particle phase of the flow may result in a significant error, as Goren[9] pointed out. Furthermore, in a heat exchanger using high temperature combustion exhaust gas, this effect should be taken into account. Nevertheless, the only analysis of thermophoresis for absorbing, emitting particles has been performed for absorbing particles. Thus the main purpose of the present study is to analyze qualitatively the radiative effect of properly loaded highly absorbing, emitting particles in gas streams on thermophoretic particle transport.

The present study is limited to one-way coupling; that is, the particle movement does not affect the gas flow. One-way coupling may be assumed when the particle mass loading is not high.[15] In this situation, all the governing equations of a two-phase flow system are uncoupled in the numerical computation. In contrast, radiation is coupled with forced convection through the energy conservation equation, which includes the

Address reprint requests to Dr. Kim at the Department of Mechanical Engineering, Korea Advanced Institute of Science and Technology, P.O. Box 150, Cheong Ryang, Seoul 130-650, Korea.

Received 1 June 1989; accepted 20 December 1989

divergence of radiative flux. Finally, a parametric study is conducted using dimensionless variables, such as optical length τ_o and ratio of conduction to radiation N. Our main purpose is not to analyze a specific system but to investigate qualitatively the effect of radiative heat transfer on the thermophoresis phenomenon.

Governing equations

The present study treats a dilute gas–particle flow that neglects the stress tensor (momentum transfer by diffusion) caused by the infrequent interaction between suspended particles (i.e., $\tau_A/\tau_c < 1$).[16] A two-fluid model is used, since it can be easily applied to a multidimensional flow system. This model also provides a rational framework that can be extended to high mass loading. The theoretical analysis of the thermophoresis phenomenon yields the following expression for thermophoretic velocity[9]:

$$v_T = -\frac{vK}{T}\nabla T \tag{1}$$

where K is the dimensionless thermophoretic coefficient. It depends on the regime of flow past the particle described in terms of the Knudsen number ($\mathrm{Kn} = \lambda/(d_p/2)$), which represents the ratio of molecular mean free path to particle size. For the transition regime, where the molecular mean free path is on the order of the particle radius, Derjaguin *et al.*[6] give the following expression:

$$K = K_t \frac{1 + C_t[\lambda/(d_p/2)](K_p/K_g)}{1 + K_p/(2K_g) + C_t[\lambda/(d_p/2)](K_p/K_g)} \tag{2}$$

where C_t is the temperature jump coefficient in the Smoluchowski formula, and K_t is the thermal slip coefficient. The values of these coefficients are 2.16 and 1.17, respectively. The results of Derjaguin *et al.* were in good agreement with the experimental data for the thermophoretic coefficient K, ranging from about 0.25 to 1.25 for different types of aerosol particles.

For simplicity, the following assumptions are made in the present investigation.

(1) Flow is a dilute gas–particle flow owing to the low particle mass loading.
(2) For the gas phase of the flow, the flow field is hydrodynamically fully developed; for the particle phase, the same flow field is assumed at the pipe inlet.
(3) Temperature and particle concentration distributions are uniform at the pipe inlet.
(4) Fluid and particle properties are independent of temperature.
(5) The pipe wall is isothermal and gray.
(6) The gas is transparent to radiation and the solids are

Notation

C_L Thermal loading ratio ($=\rho_p c_{pp}/\rho_g c_{pg}$)
c_{pg} Heat capacity of gas
c_{pp} Heat capacity of particle
C_t Temperature jump coefficient
D Tube diameter
d_p Particle diameter
$E(x)$ Cumulative collection efficiency defined in Equation 13
G_0, G_o Dimensionless zeroth-order moment of intensity
I_0 Zeroth-order moment of intensity
J_p Particle deposition flux
K Thermophoretic coefficient
K_g Conductivity of gas
K_p Conductivity of particle
K_t Thermal slip coefficient
N Ratio of conduction to radiation
n Refractive index
n_p Number of particles per unit volume
Pe Peclet number ($=\mathrm{RePr}$)
Pe_R Peclet number ($=\mathrm{Re}_R\mathrm{Pr}$)
Pr Prandtl number
R Tube radius
Re Reynolds number ($=U_{\mathrm{avg}}D/\nu$)
Re_R Reynolds number ($=U_{\mathrm{avg}}R/\nu$)
r Radial coordinate
Stk Stokes number $\left(=\dfrac{\rho_{pm}d_p^2 U_{\mathrm{avg}}}{18\mu R}\right)$
T Temperature
T_m Mixed mean temperature
u Velocity in the axial direction
U_{avg} Average gas velocity over the cross section in the x-direction
v Velocity in the radial direction
v_T Thermophoretic velocity
$\forall_p$ Volume of single particle
x Axial coordinate

Greek symbols
β Absorption coefficient
ε_p Particle surface emissivity
ε_w Tube surface emissivity
ϕ Dimensionless particle concentration ratio ($\rho_p/\rho_{p,\mathrm{in}}$)
η Dimensionless radial coordinate
λ Molecular mean free path
μ Dynamic viscosity of gas
ν Kinematic viscosity of gas
θ, Θ Dimensionless temperature (T/T_{in})
θ_0 Dimensionless temperature at tube inlet ($=1$)
θ_m Dimensionless mixed mean temperature (T_m/T_{in})
θ^*, Θ^* $T_w/(T_{\mathrm{in}} - T_w)$
ρ_g Gas density
ρ_p Apparent particle density
$\rho_{p,\mathrm{in}}$ Apparent particle density at tube inlet
ρ_{pm} Material density of single particle
σ Stefan–Boltzmann constant
τ_A Aerodynamic response time
τ_c Mean time between particle-to-particle collision
τ_{flow} Characteristic flow time
τ_{mom} Momentum relaxation time
τ_o, τ_0 Optical thickness
τ_T Thermal relaxation time
ξ Dimensionless axial coordinate

Subscripts
g Refers to gas phase
in Refers to tube inlet
p Refers to particle phase
w Refers to wall surface

Superscripts
$*$ Refers to dimensionless form

limited to the gray absorbing, emitting particles without scattering.
(7) The absorption coefficient is constant in the thermal field.
(8) The particles are spheres of uniform size.
(9) Particle coagulation is neglected.
(10) The gas and particle phases are at the same temperature.

The pipe and flow configurations and cylindrical coordinate system are depicted in Figure 1. The governing equations of each phase are based on a two-fluid model.

The gas-phase velocity is assumed to be fully developed and not altered by the particulate flow because of low particle mass loading. Hence the dimensionless gas velocity is given by

$$u_g = 2(1-\eta^2) \tag{3}$$

Here, u_g is made nondimensional by the average gas velocity over the cross section, U_{avg}, and η denotes the dimensionless radial coordinate of the pipe.

For the particle phase, the conservation equations can be written in a dimensionless form.

- *Mass conservation equation:*

$$\frac{\partial}{\partial \xi}(\phi u_p) + \frac{1}{\eta}\frac{\partial}{\partial \eta}(\eta \phi v_p) = 0 \tag{4}$$

- *u momentum equation:*

$$u_p \frac{\partial u_p}{\partial \xi} + v_p \frac{\partial u_p}{\partial \eta} = -\frac{1}{\mathrm{Stk}}(u_p - u_g) - \frac{1}{\mathrm{Stk}}\frac{K}{\mathrm{Re}_R}\frac{1}{\theta}\frac{\partial \theta}{\partial \xi} \tag{5}$$

- *v momentum equation:*

$$u_p \frac{\partial v_p}{\partial \xi} + v_p \frac{\partial v_p}{\partial \eta} = -\frac{1}{\mathrm{Stk}}(v_p - v_g) - \frac{1}{\mathrm{Stk}}\frac{K}{\mathrm{Re}_R}\frac{1}{\theta}\frac{\partial \theta}{\partial \eta} \tag{6}$$

where

$$\xi = \frac{x}{R} \qquad \eta = \frac{r}{R} \qquad \phi = \frac{\rho_p}{\rho_{p,\mathrm{in}}} \qquad \theta = \frac{T}{T_{\mathrm{in}}}$$
$$\mathrm{Re}_R = \frac{U_{\mathrm{avg}} R}{\nu} \quad \text{and} \quad \mathrm{Stk} = \frac{\rho_{pm} d_p^2 U_{\mathrm{avg}}}{18\,\mu R} \tag{7}$$

The particle velocity components u_p and v_p are normalized by U_{avg}; ρ_p denotes the apparent density of dispersed particles, defined as $\rho_p = \rho_{pm} n_p v_p$. The Stokes number represents the ratio of the momentum relaxation time τ_{mom} to the characteristic flow time τ_{flow}.[16] If the Stokes number is very small, the particles will move with the host fluid in the same manner. Similarly, τ_{mom} coincides with the thermal relaxation time τ_T when the Prandtl number is 2/3.[17] The present calculation uses Pr = 2/3.

The boundary conditions for Equations 4, 5, and 6 are given by

$$u_p = u_g \qquad v_p = 0 \quad \text{and} \quad \phi = 1 \qquad \text{at } \xi = 0$$
$$\frac{\partial u_p}{\partial \eta} = v_p = \frac{\partial \phi}{\partial \eta} = 0 \qquad \text{at } \eta = 0 \tag{8}$$

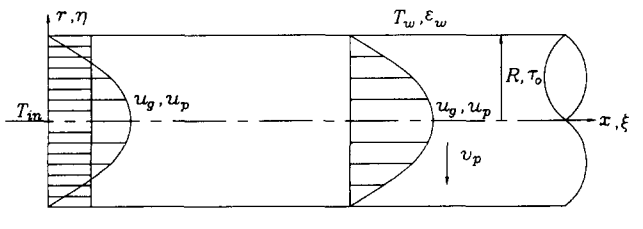

Figure 1 Cylindrical coordinate system

Mixture energy equation

For small τ_T and τ_{mom}, the energy conservation equations of each phase may be combined into a mixture energy equation. In terms of dimensionless variables, the mixture energy equation can be written as[18]

$$(1 + C_L)u_g \frac{\partial \theta}{\partial \xi} = \frac{1}{\mathrm{Pe}_R}\frac{\partial^2 \theta}{\partial \xi^2} + \frac{1}{\mathrm{Pe}_R}\frac{1}{\eta}\frac{\partial}{\partial \eta}\left(\eta \frac{\partial \theta}{\partial \eta}\right) - \frac{\tau_o^2}{\mathrm{Pe}_R N}(\theta^4 - G_o) \tag{9}$$

where

$$C_L = \frac{\rho_p c_{pp}}{\rho_g c_{pg}} \qquad \theta = \frac{T}{T_{\mathrm{in}}} \approx \frac{T_g}{T_{\mathrm{in}}} \approx \frac{T_p}{T_{\mathrm{in}}} \qquad \mathrm{Pe}_R = \mathrm{Re}_R \mathrm{Pr}$$
$$\tau_o = \beta R \qquad N = \frac{K_g \beta}{4\sigma n^2 T_{\mathrm{in}}^3} \quad \text{and} \quad G_0 = \frac{I_0}{4\sigma n^2 T_{\mathrm{in}}^4} \tag{10}$$

The last term in the right-hand side of Equation 9 represents the divergence of radiative heat flux; G_0 denotes incident radiation; and N and τ_o are the dimensionless variables that denote the ratio of conduction to radiation and the optical radius, respectively.

We adopted the P-1 approximation for the solution of the radiative transfer equation to obtain G_0.[19] Actually, the P-1 approximation poorly predicts the radiative heat transfer in an optically thin situation.[19] However, it may describe qualitatively, at least, the effect of radiative heat transfer on the thermophoretic particle transport. The tube surface emissivity is taken as 0.7 in the present study.

The boundary conditions are

$$\theta = 1 \qquad \text{at } \xi = 0$$
$$\frac{\partial^2 \theta}{\partial \xi^2} = 0 \qquad \text{at exit}$$
$$\frac{\partial \theta}{\partial \eta} = 0 \qquad \text{at } \eta = 0 \tag{11}$$
$$\theta = \theta_w \qquad \text{at } \eta = 1$$

The particle deposition flux at the wall may be expressed as

$$J_p = \phi v_p|_w \tag{12}$$

Also, the cumulative collection efficiency is defined as the percentage of particles that are deposited on the wall within a distance x from the tube inlet.[12]

$$E(x) = \frac{\int_0^x J_p(s) 2\pi\, ds}{\phi_{\mathrm{in}} U_{\mathrm{avg}} \pi R} \tag{13}$$

Results and discussion

In order to check the accuracy of the present numerical method, we compared the results with the solutions by Walker *et al.*[12] and Pearce and Emery.[20] We obtained the present numerical solutions for the energy equation by line SOR solver, utilizing the power law differencing scheme[21] and the upwind scheme for particle transport.[22] As shown in Figure 2, in the absence of radiation, the cumulative collection efficiency resulting from thermophoretic particle transport agree well with Walker's results. It seems that the slight disagreement is caused by the difference in solution methods. Walker used a particle trajectory model,[12] but we adopted the Eulerian approach.

Figure 3 shows that P-1 approximation solutions for the coupled energy equation involving the radiative flux agree closely with Pearce and Emery's results.[20] In Figures 4–11, we presented the solutions in terms of the optical radius τ_0 and the conduction-to-radiation parameter N.

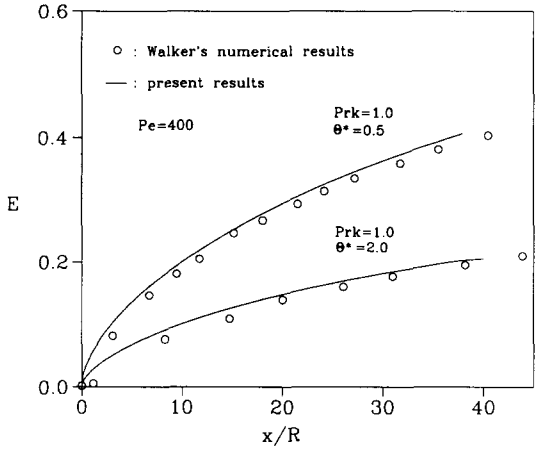

Figure 2 Cumulative collection efficiency along axial dimension for different operating conditions

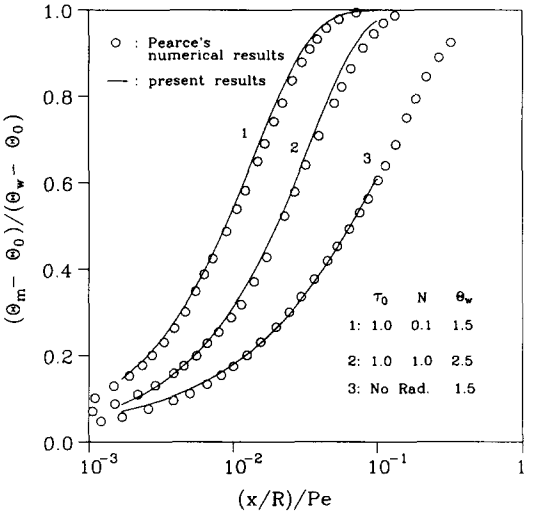

Figure 3 Mean temperature versus $(x/R)/\mathrm{Pe}$

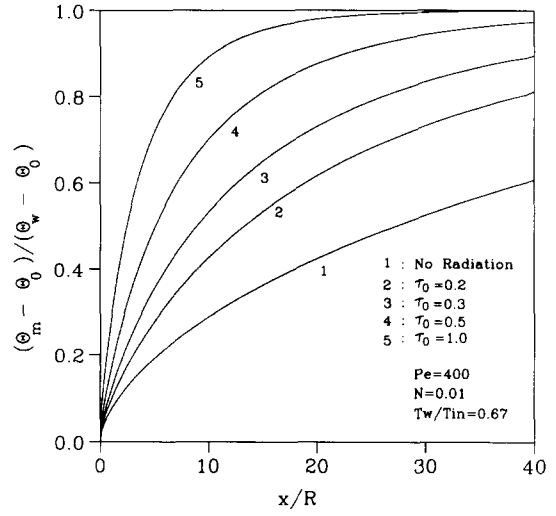

Figure 4 Mean temperature along axial dimension (effect of τ_0)

In Figure 4, the mixed mean temperature distributions along the axial dimension are depicted with the variation of τ_0 at $N=0.01$. Because of the nonlinear source term in Equation 9, the solution procedures are iterative in nature. In particular,

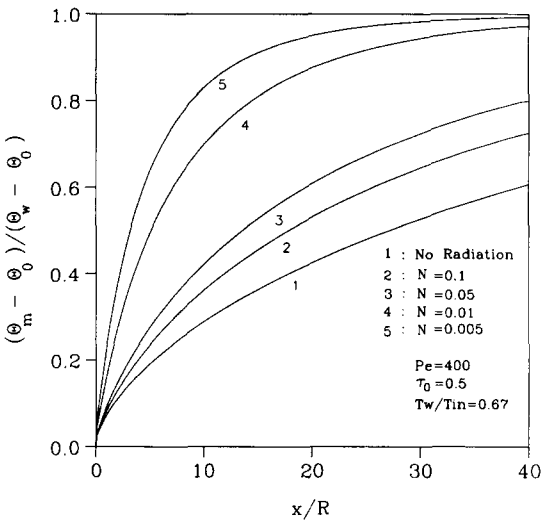

Figure 5 Mean temperature along axial dimension (effect of N)

with an increase in τ_0, the mean temperature approaches the wall temperature asymptotically more rapidly. The attenuation of the emitted radiant energy (by the wall) is much stronger for the larger values of the optical radius. Hence we expect the thermal entry length to become shorter.

In Figure 5, the results are given in terms of the conduction-to-radiation parameter N at $\tau_0=0.5$. For smaller N, radiation becomes dominant, contributing to more rapid thermal development. Over the axial distance $x/R=10$, the mixed mean temperature nearly approaches the wall temperature when N is smaller than 0.01.

Figure 6 shows the effect of radiation, with the variation of τ_0, on particle diffusion velocity in the case of $T_w/T_{in}=0.67$, $\theta^*=2.0$. This drift velocity is dominated by the fully known source term in the momentum equations for the particle phase. As expressed in Equations 1 and 2, particle diffusion velocity depends strongly on the Knudsen number in relation to particle size and the temperature gradient. The thermophoretic coefficient K from Derjaguin's expression may be obtained under the condition of $d_p=0.4\,\mu$m in submicron size, neglecting the inertial transport mechanism. At $\tau_0=0$, as the particle moves downstream, its diffusion velocity decreases slightly near the wall and increases far from the wall. With an increase in the optical radius τ_0 near the entrance region ($x/R=10$), the radial component v_p becomes slightly larger than that of $\tau_0=0$ in the tube core region. Neglecting radiation, we find that heat transfer occurs only through the diffusion process, and hence the thermal boundary layer is confined in the vicinity of the wall. However, when radiation is present—because of its far-reaching nature—the temperature gradient may exist even in the core region. In addition, in the case of strong radiation ($\tau_0=1.0$), there is no particle transport in the core region, since the temperature profile becomes flat except in the conduction region near the wall.

Figure 7 gives a series of concentration profiles at three axial distances, $x/R=10$, $x/R=25$, and $x/R=40$, for various optical radii at $T_w/T_{in}=0.67$ and $N=0.01$. As shown, near the wall surface the particle concentration abruptly drops with an increase in τ_0, and thus the concentration boundary layer becomes thinner. In the streamwise direction, the difference in the particle concentration between the various τ_0's increases, except for the conduction region, as expected from Figure 6. In addition, for smaller τ_0's the concentration ϕ tends to decrease along the axial dimension, because of the cumulative deposition to the wall by the thermophoretic effect, until the

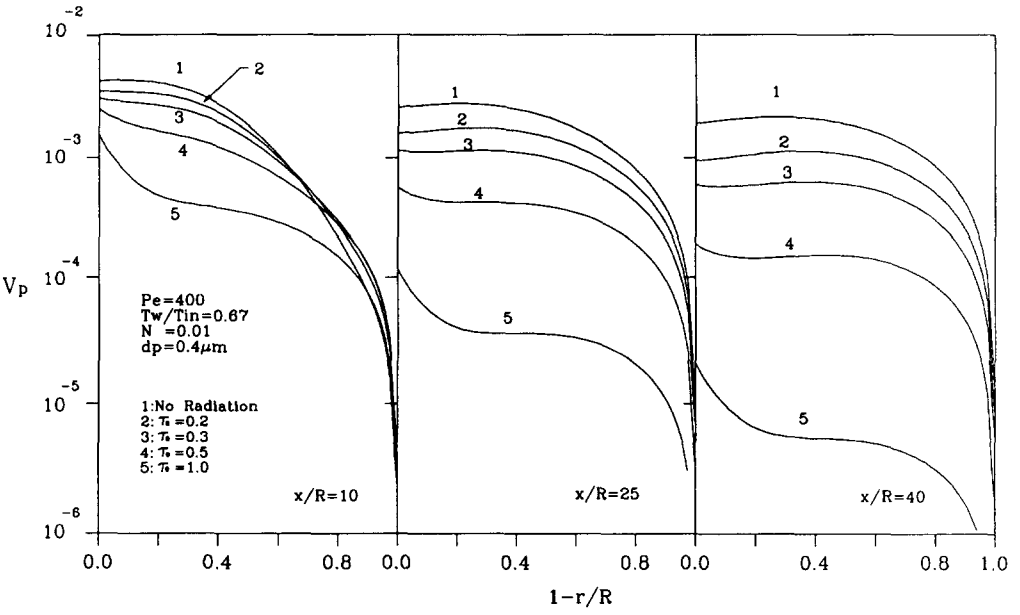

Figure 6 Particle diffusion velocity profiles at arbitrary axial distances (effect of τ_0)

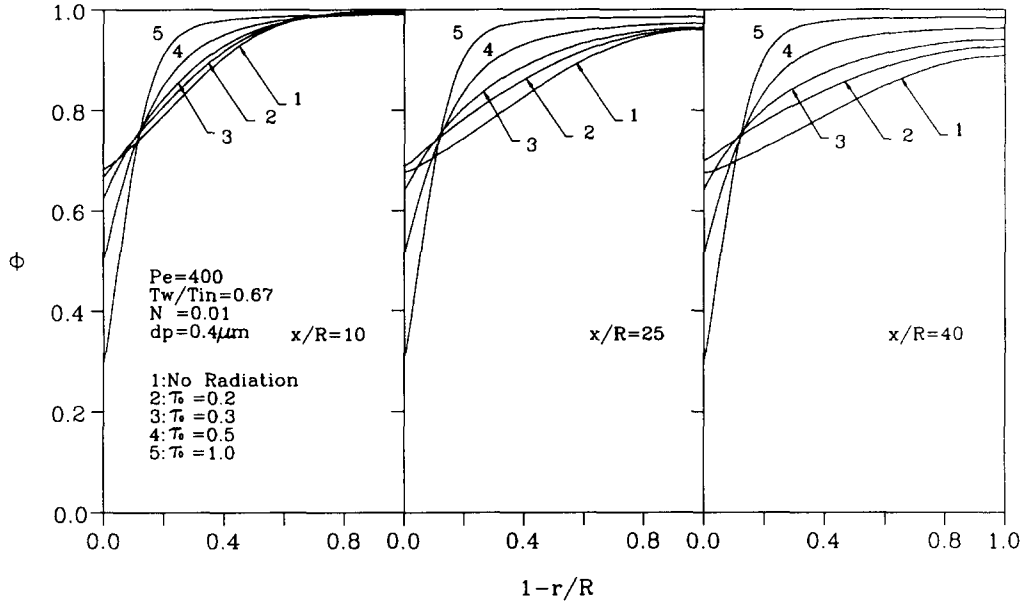

Figure 7 Particle concentration profiles at arbitrary axial distances (effect of τ_0)

fluid temperature equilibrates with the wall temperature at $x/R=40$. Thus we would expect much more difference in ϕ between the τ_0's. In fact, higher overall particle concentration over the tube cross section, except for the vicinity of the wall, is obtained from larger radiation effects. As shown in Figure 7, particle concentration is not distributed uniformly for various τ_0, so the present assumption of a uniform absorption coefficient in all thermal fields may not be valid. However, this assumption is considered sufficient for investigating the qualitative trend, while avoiding the complexity of concentration dependence on the radiative property.

Figure 8 shows the effect of τ_0 and N on the cumulative collection efficiency $E(x)$ along the axial dimension. The thermophoretic particle flux can be obtained from the particle diffusion velocity and concentration at the wall. With an increase in τ_0, $E(x)$ more quickly reaches some constant value asymptotically. At $x/R=40$, the cumulative collection efficiency for larger τ_0's becomes considerably lower than that of "no radiation." We expect it to be much lower farther downstream.

Figure 9 shows a trend similar to that of Figure 8: a remarkable decrease in $E(x)$ below $N=0.01$ compared to that of "no radiation." In a gas–particle suspension flow system, the hydraulic radius and mass loading ratio should be enlarged, even for the weakly radiating medium, and particulates with a high surface emissivity should be used in order to obtain a low $E(x)$ as prescribed in the absorption coefficient $\beta=\pi(d_p/2)^2 n_p \varepsilon_p$.[23]

Figure 10 shows the effect of thermal loading ratio C_L on $E(x)$ at $\tau_0=0.5$ and $N=0.01$. The larger values of C_L are obtained by increasing the product of ρ_p and c_{pp} as N, τ_0, and Pe are held constant. Clearly, an increase in C_L (holding N, τ_0, and Pe constant) results in a decrease in the development

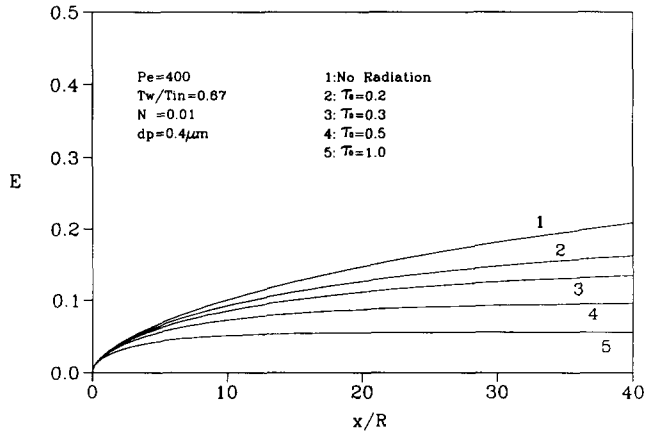

Figure 8 Cumulative collection efficiency along axial dimension (effect of τ_0)

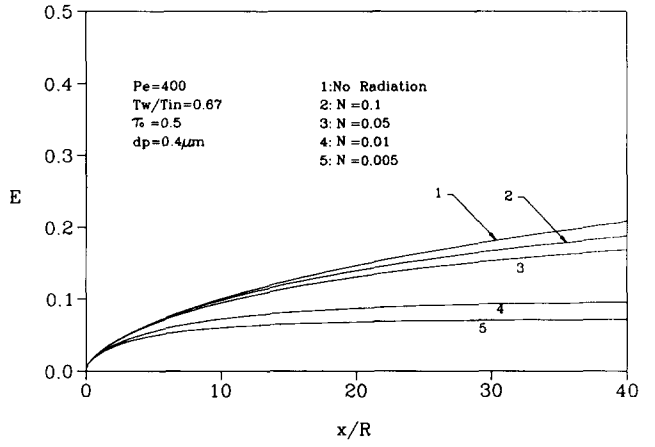

Figure 9 Cumulative collection efficiency along axial dimension (effect of N)

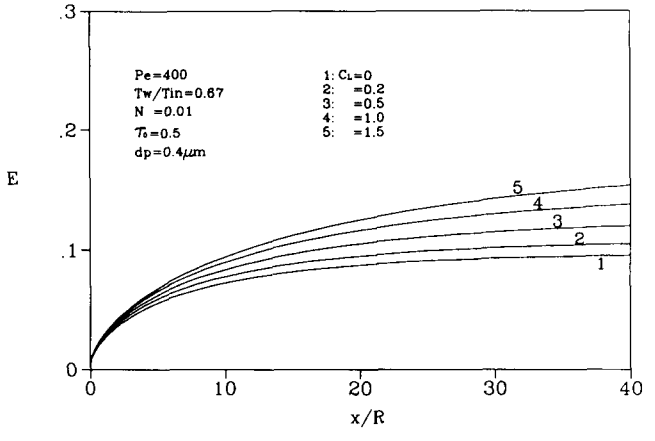

Figure 10 Cumulative collection efficiency for various thermal loading ratios

rate of the temperature profile; thus the temperature gradient near the wall increases, as does the cumulative collection efficiency (as $\rho_p c_{pp}$ increases). Because $E(x)$ varies significantly with C_L, the effect of the thermal loading ratio should be taken into account when $C_L > 0.2$ in the evaluation of $E(x)$.

Figure 11 shows the effect of the Stokes number on $E(x)$. Variations in the Stokes number for constant particle size ($d_p = 1$ μm) are considered despite the strong dependence of Stk

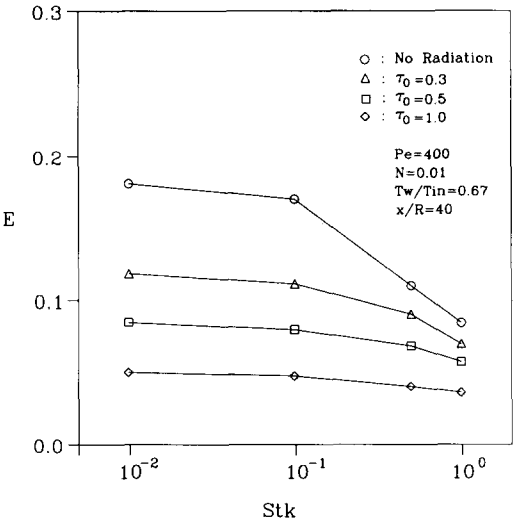

Figure 11 Cumulative collection efficiency versus Stokes number for various τ_0

on particle size. The decline in efficiency occurs at or near Stk = 0.1 in all cases. In the case of "no radiation," $E(x)$ drops steeply near Stk = 0.1, whereas a gradual decrease is suggested for larger τ_0's. In particular, a smaller rate of decline in $E(x)$ is obtained at larger τ_0's. It is also notable that, for $\tau_0 = 1.0$, the efficiency remains nearly constant.

Conclusions

In a nonisothermal fluid field, thermophoresis is a dominant mechanism for particle diffusion for low Stokes numbers. Several important observations are noted and summarized below. In the absence of confirming experimental evidence, the observations are mainly of qualitative value.

(1) With a strong radiative contribution, the concentration boundary layer becomes thin because of a much smaller value of the particle diffusion velocity far from the wall, compared to that without radiation.

(2) As expected from the particle concentration and drift velocity distribution, the cumulative collection efficiency becomes considerably smaller when highly absorbing, emitting particles are present under the proper loading condition. Additionally, at high or extremely high gas temperature, a similar result is obtained.

(3) When the thermal loading ratio at fixed τ_0 increases, the cumulative collection efficiency becomes larger. Meanwhile, an increase in C_L resulting from a higher particle volume fraction leads to deceleration of the effect of the thermal loading ratio on the thermophoresis phenomenon because of the increasing radiative effect corresponding to larger τ_0.

(4) At or near the critical Stokes number (=0.1), the rate of decrease for the cumulative collection efficiency $E(x)$ becomes larger; that is, because of the inertial transport mechanism in parallel-flow systems, the thermophoretic effect on the deposition of particles to the cold wall is reduced. Moreover, this behavior becomes significant in the absence of radiation but is less important as the radiative effect increases.

References

1 Batchelor, G. K. and Shen, C. Thermophoretic deposition of particles in gas flowing over cold surfaces. *J. Colloid and Interface Science*, 1985, **107**(1), 21–37

2 Narsimhan, G. and Ruckenstein, E. Monte Carlo simulation of Brownian coagulation over the entire range of particle sizes from near molecular to colloidal: Connection between collision efficiency and interparticle forces. *J. Colloid and Interface Science*, 1985, **107**(1), 174–193

3 Friedlander, S. K. *Smoke, Dust and Haze*. Wiley-Interscience, New York, 1977

4 Pratsinis, S. E. and Kim, K. Particle coagulation, diffusion and thermophoresis in laminar tube flows. *J. Aerosol Sci.*, 1989, **20**(1), 101–111

5 Fulford, G. D., Moo-Young, M., and Bebu, M. Thermophoretic acceleration of particle deposition from laminar air streams. *Canad. J. Chem. Eng.*, 1971, **49**, 553–556

6 Derjaguin, B. V., Rabinovich, Ya. I., Storozhilova, A. I., and Shcherbina, G. I. Measurement of the coefficient of thermal slip of gases and the thermophoresis velocity of large-size aerosol particles. *J. Colloid and Interface Science*, 1976, **57**, 451–461

7 Goldsmith, P. and May, F. G. *Aerosol Science*. Academic Press, New York, 1966

8 Rosner, D. E. and Kim, S. S. Optical experiments on thermophoretically augmented submicron particle deposition from "Dusty" high temperature gas flows. *Chem. Eng. J.*, 1984, **29**, 147–157

9 Goren, S. L. Thermophoresis of aerosol particles in the laminar boundary layer on a flat plate. *J. Colloid and Interface Science*, 1977, **61**(7), 77–85

10 Calvert, S. and Byers, L. J. *Air Pollution Control Assoc.*, 1967, **17**, 595

11 Epstein, M., Hauser, G. M., and Henry, R. E. Thermophoretic deposition of particles in natural convection flow of a vertical plate. *ASME J. Heat Transfer*, 1985, **107**, 272–276

12 Walker, K. L., Homsy, G. M., and Geyling, F. T. Thermophoretic deposition of small particles in laminar tube flow. *J. Colloid and Interface Science*, 1979, **69**(1), 138–147

13 Morse, T. F., Wang, C. Y., and Cipolla, Jr., J. W. Laser-induced thermophoresis and particulate deposition efficiency. *ASME J. Heat Transfer*, 1985, **107**, 155–160

14 Cipolla, Jr., J. W. and Morse, T. F. Thermophoresis in an absorbing aerosol. *J. Aerosol Science*, 1987, **18**(3), 245–260

15 Lee, J. S. and Humphrey, J. A. C. Radiative-convective heat transfer in dilute particle-laden channel flows. *Physico Chemical Hydrodynamics*, 1986, **7**(5/6), 325–351

16 Crowe, C. T. Review—Numerical methods for dilute gas-particle flow. *ASME J. Fluids Engineering*, 1982, **104**, 297–303

17 Marble, F. E. Dynamics of dusty gases. *Ann. Review, Fluid Mech.*, 1970, **2**, 397–446

18 Tabanfar, S., and Modest, M. F. Combined radiation and convection in absorbing, emitting, nongray gas-particulate tube flow. *ASME J. Heat Transfer*, 1987, **109**, 478–484

19 Menguc, M. P. and Viskanta, R. Radiative transfer in axisymmetric finite cylindrical enclosures. *ASME J. Heat Transfer*, 1986, **108**, 271–276

20 Pearce, B. E. and Emery, A. F. Heat transfer by thermal radiation and laminar forced convection to an absorbing fluid in the entry region of a pipe. *ASME J. Heat Transfer*, 1970, **92C**, 221–230

21 Patankar, S. V. *Numerical Heat Transfer and Fluid Flow*. McGraw-Hill, New York, 1980

22 Roache, P. J. *Computational Fluid Dynamics*. Hermosa, Albuquerque, 1976

23 Echigo, R., Hasegawa, S., and Tamehiro, H. Radiative heat transfer by flowing multiphase medium—Part II. An analysis on heat transfer of laminar flow in an entrance region of circular tube. *Int. J. Heat Mass Transfer*, 1972, **15**, 2595–2610